Distorted Pacific-North American Teleconnection at the Last Glacial Maximum

Yongyun Hu[1*], Yan Xia[1], Zhengyu Liu[1,2], Yuchen Wang[1], Zhengyao Lu[1], and Tao Wang[3]

[1]Laboratory for Climate and Ocean-Atmosphere Studies, Department of Atmospheric and Oceanic Sciences, School of Physics, Peking University, Beijing 100871, China

[2]Atmospheric Science Program, Department of Geography, Ohio State University, Columbus, OH, 43210, USA

[3]Nansen-Zhu International Research Centre, Institute of Atmospheric Physics, Chinese Academy of Sciences, Beijing 100029, China

Corresponding author: Yongyun Hu, email: yyhu@pku.edu.cn

Abstract

The Pacific-North American (PNA) teleconnection is one of the most important climate modes in the present climate condition, and it enables climate variations in the tropical Pacific to exert significant impacts on North America. Here, we show climate simulations that the PNA teleconnection was largely distorted or broken at the Last Glacial Maximum (LGM). The distorted PNA is caused by a split of the westerly jet stream, which is ultimately forced by the thick and large Laurentide ice sheet at the LGM. Changes in the jet stream greatly alter the extratropical wave guide, distorting wave propagation from the North Pacific to North America. The distorted PNA suggests that climate variability in the tropical Pacific, notably, El Niño and Southern Oscillation (ENSO), would have little direct impact on North American climate at the LGM.

1 Introduction

The Pacific-Northern-American (PNA) teleconnection is the major atmospheric teleconnection mode that links climate variations from the tropical Pacific to North America for the present-day climate state (Horel and Wallace, 1981; Wallace and Gutzler, 1981). Especially, climate variability associated with El Niño and Southern Oscillation (ENSO) exerts great impacts on the North American climate through the PNA teleconnection (Henderson and Robinson, 1994; Lau, 1997; Leathers et al., 1991; Straus and Shukla, 2002). It is well known that the PNA is largely constrained by extratropical atmospheric flows, notably, the extratropical wave guide (Held, 1983; Held et al., 2002; Hoskins and Karoly, 1981; Jin and Hoskins, 1995). Thus, changes in extratropical atmospheric flows should alter the PNA under different climate conditions.

It has been shown that greenhouse warming leads to a strengthening and a shift of the PNA due to altered extratropical atmospheric flows (Allan et al., 2014; Chen et al., 2017). There has also been a large body of works that demonstrated significant differences in extratropical atmospheric circulations in cold climates, notably, the Last Glacial Maximum (LGM). It was shown that during the LGM the Aleutian low pressure system was enhanced in winter, the Pacific high pressure system was weakened in summer (Yanase and Abe-Ouchi, 2007; Yanase and Abe-Ouchi, 2010), the westerly jet shifted southward (Braconnot et al., 2007; Otto-Bliesner et al., 2006), and transient waves were weakened over the North Pacific and strengthened over the North Atlantic (Justino and Peltier, 2005; Justino et al., 2005). These works suggest that the PNA could be changed for different climate regimes. Therefore, a natural question is whether the PNA is also significantly altered due to atmospheric circulation changes at the LGM.

The LGM occurred between 23,000 and 19,000 years ago (Clark et al., 2009; Clark and Mix, 2002). One of the most significant climatic characteristics at LGM is the maximum expansion of mid-latitude ice sheets. Extensive ice sheets grew over North America and northwestern Europe, with the Laurentide ice sheet over North America, in particular, of an ice thickness of 3 to 4 kilometers (Marshall et al., 2002). Early simulations have shown that the thick and large Laurentide ice sheet forced a split of the extratropical westerly jet stream into the northern and southern branches (Cohmap, 1988; Kutzbach and Wright, 1985; Rind, 1987), and that the jet split leads to regional climate changes over the globe, especially over North America. Proxy records showed that there were more storms and precipitation associated with the southern branch, causing high lake levels and increased woodlands in the southwestern United States (Cohmap, 1988; Kutzbach and Wright, 1985).

Recent modeling studies showed that the Arctic Oscillation and storm tracks at LGM differ significantly from the present (Justino and Peltier, 2005; Laîné et al., 2009; Li and Battisti, 2008; Lü et al., 2010; Rivière et al., 2010), and that the Laurentide ice sheet can also influence the Southern-Hemisphere atmospheric teleconnection and climate variability over West Antarctic (Jones et al., 2018). Therefore, it is possible that changed atmospheric circulations at LGM might also significantly alter the PNA and thus climate linkage between the tropical Pacific and North America.

In the present paper, using climate simulation results, we show that the PNA is largely distorted or even broken by the Laurentide ice sheet at LGM, and that ENSO had little direct impact on North American climates. We will also address how the PNA is altered by the Laurentide ice sheet.

2 Models and data

The simulation results from the Paleoclimate Modeling Intercomparison Project 2 (PMIP2) (Braconnot et al., 2012; Braconnot et al., 2007) and 3 (PMIP3) (Abe-Ouchi et al., 2015) are utilized in this study. By comparing the PNA patterns in the Preindustrial condition (PIC) with LGM simulations as well as our own sensitivity simulations, the changes in the PNA pattern at LGM are identified. The horizonal resolution of the models we use are listed in table S1. For comparison, we also use the NCEP/NCAR reanalysis data from 1988 to 2017 (Kistler et al., 2001), with horizontal resolution of $2.5^{\circ} \times 2.5^{\circ}$. We shall mainly focus on the simulation results from the Community Climate System Model version 3 (CCSM3) (Collins et al., 2006; Jones et al., 2018; Otto-Bliesner et al., 2006; Yeager et al., 2006), since our sensitivity simulations are performed with the same model.

To understand the impact of the topography of the Northern-Hemisphere glacial ice sheets on the PNA, we performed a series of sensitivity simulations with different ice sheet thicknesses, which are 0%, 20%, 40%, 60%, 80%, 100%, and 150% of the ice sheet thickness that was used in PMIP2. Note that different ice sheet reconstructions were used in PMIP2 and PMIP3 simulations. PMIP2 simulations used the ICE-5G (VM2) reconstruction (Peltier, 2004), while PMIP3 simulations used the ICE-6G reconstruction. In general, the ice sheet thickness in ICE-6G reconstruction is approximately equal to 80% of ICE-5G for most parts of the North American region (Figure S1). In our sensitivity simulations, the case of 0% ice sheet thickness means that the thickness of the ice sheet is set to zero, but the surface albedo remains ice albedo. All other conditions are the same as that in the LGM simulations of PMIP2. The model for our sensitivity simulations is a lower-resolution version of CCSM3 (T31), with horizontal a resolution of $3.8^{\circ} \times 3.8^{\circ}$. It differs from the PMIP2 models (T42), with a horizontal resolution of $2.8^{\circ} \times 2.8^{\circ}$. Although the horizontal resolution in CCSM3 T31 is lower, it can well reproduce the present-day PNA pattern in the PIC simulation, consistent with the results in Magnusdottir and Haynes (1999) and Löfverström et al. (2016). Therefore, the results here are not sensitive to model resolutions.

Following Horel and Wallace (1981) and Wallace and Gutzler (1981), the PNA teleconnection is characterized by the pointwise correlation method. The four base points that represent the centers of action are located near Hawaii (20°N, 160°W), North Pacific (45°N, 165°W), Alberta (55°N, 115°W), and the Gulf Coast (30°N, 85°W), respectively. The four base points were objectively derived with teleconnectivity analysis (Sherriff-Tadano and Itoh, 2013; Wallace and Gutzler, 1981). To examine whether models can reasonably simulate the PNA in PIC simulations and whether the PNA pathway is altered in LGM simulations, we loosely define a circular region around each of the centers of North Pacific, North America and the Gulf Coast (the base point is near Hawaii), with a radius of 10 degrees. For PIC simulations, if a model cannot generate statistically significant correlations (coefficients greater than 0.35) within the circular regions, the model is considered to have poor performance in simulating PNA. For these models with good performance in simulating PNA their PIC simulations, if their LGM simulations shows absence of significant correlations in the three circular regions, the PNA pathway is considered to be distorted or broken at LGM. Because the PNA is most active in DJF, our analysis below will mainly focus on the December-January-February (DJF) season.

In the present paper, all correlation analyses are conducted with monthly-mean model outputs of the last 30-year simulations. Correlation coefficient 0.35 corresponds to the 95% confidence level for 30-year correlations.

3 Results

Fig. 1 shows one-point correlation maps of 500 hPa geopotential heights in DJF, with the base point near Hawaii. The correlation maps in Figs. 1a and 1b exhibit similar wave-train patterns, with centers of positive and negative correlations extending from Hawaii to North Pacific, Alberta, and finally to the Gulf Coast, respectively. Hence, the present-day PNA is reproduced reasonably well in CCSM3. In contrast, this PNA pattern is altered dramatically in the LGM simulation of CCSM3 (Fig. 1c). The negative correlation over North Pacific is reduced, and the center of positive correlation is rather weak and shifted to the Arctic. The most striking feature in Fig. 1c is that the center of negative correlation near the Gulf Coast completely disappears. The results in Fig. 1 indicate that the PNA teleconnection is largely distorted at LGM. This is the most important point of the present paper.

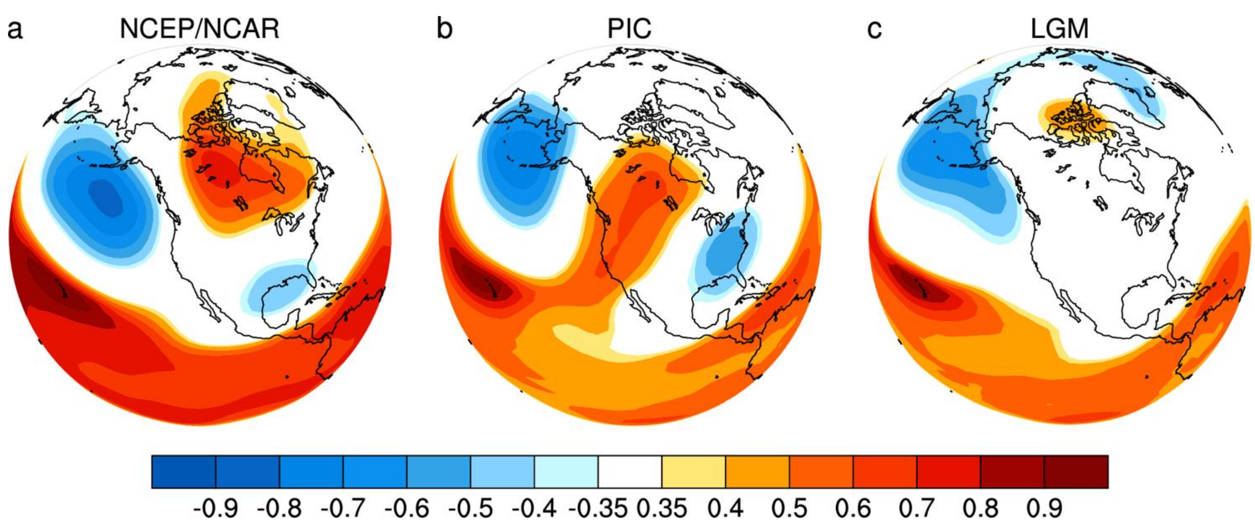

Fig. 1. One-point correlation maps of 500 hPa geopotential heights in DJF in NCEP/NCAR reanalysis and PMIP2 CCSM3 simulations. (a) NCEP/NCAR, (b) PIC, and (c) LGM. The base point is near Hawaii. The correlation coefficient of 0.35 corresponds to the 95% confidence level for 30-year correlations.

This distorted PNA at LGM can also be seen from correlation maps for the other three base points. When the base point is located over North Pacific (Fig. S2c), the center of positive correlation over North America is shifted to northern Canada. For the base point over North

America (Fig. S2f), the negative correlations over North Pacific and the Gulf Coast are all largely reduced, and the center of positive correlation near Hawaii disappears. This result indicates a disconnection between North America and the tropical Pacific. For the base point near the Gulf Coast (Fig. S2i), a wave train is established from North Pacific to the Gulf Coast, while the center of positive correlation over North America is largely reduced, and the center of positive correlation near Hawaii is absent.

The PNA teleconnection at LGM is even completely broken in other PMIP2 models. There are seven PMIP2 models that have simulations available online. According to our definition, CCSM3, ECBILTCLIO, HadCM3M2, and CNRM-CM33 can reasonably reproduce the PNA in their PIC simulations (Fig. 1b and Figs. S3a-c), whereas IPSL-CM4-V1-MR, FGOALS-1.0g, and MIROC3.2 have poor performance. In LGM simulations, the center of negative correlation over North Pacific still exists in ECBILTCLIO, HadCM3M2, and CNRM-CM33 (Figs. S3d-f), although they all shift away from the North Pacific base point and are largely reduced. However, the center of positive correlation over North America completely disappears in these plots. Moreover, the center of negative correlation near the Gulf Coast also disappears in the three models.

PMIP3 simulations are also used to demonstrate the changes in the PNA teleconnection at LGM. There are eight PMIP3 models that have LGM simulations available online. Again, according to our definition, CCSM4, MRI-CGCM3, and MIROC-ESM can reasonably reproduce the PNA in their PIC simulations (Figs. S4a-c). The LGM simulations of CCSM4 and MRI-CGCM3 show the absence of the center of positive correlation over North America (Figs. S4d and e). The center of positive correlation in MIROC-ESM is weak and biased toward the Arctic (Fig. S4f). The center of negative correlation near the Gulf Coast is absent in MRI-CGCM3 and

MIROC-ESM. Although there is a negative center in CCSM4 (Fig. S4d), it is more like a result of the subtropical wave train, rather than a part of PNA. Thus, the LGM simulations in PMIP3 models demonstrate that the PNA is either distorted or completely broken.

We have also done Empirical Orthogonal Function (EOF) and rotated EOF (REOF) analysis to examine the PNA pattern for both LGM and PIC simulations (figures not shown here). It is found that the second REOF modes in both the NCEP reanalysis and the CCSM3 PIC simulation all well represent the loading pattern of the present-day PNA. However, the second REOF in the CCSM3 LGM simulation does not show the PNA pattern. The third and fourth REOFs in the LGM simulation show teleconnections between North Pacific and Arctic as well as between North Pacific and the southern part of North America.

Fig. 2 illustrates PNA responses to different ice sheet thicknesses in sensitivity simulations. The PNA pattern remains for ice sheet thicknesses no more than 60% of that in PMIP2 (Figs. 2a-d). In contrast, the PNA is distorted as ice sheet thickness is increased to 80%. The center of positive correlation is shifted to the Arctic, and the center of negative correlation near the Gulf Coast disappears (Fig. 2e). As ice sheet thickness is further increased to 100 % and 150% (Figs. 2f-g), the center of positive correlation over North America disappears. Again, the center of negative correlation is more like a part of the subtropical wave train. These results of sensitivity simulations suggest that the PNA is distorted or even broken as the Laurentide ice sheet is sufficiently thick.

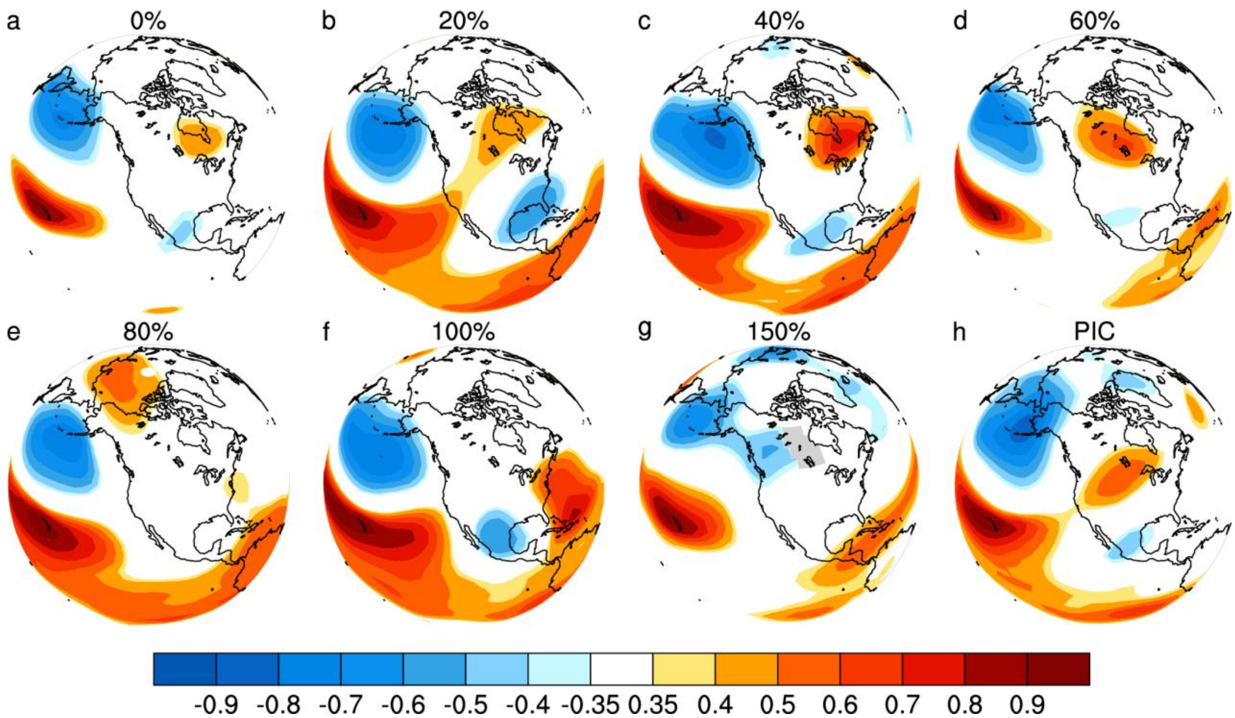

Fig. 2. One-point correlation maps of 500 hPa geopotential heights in DJF in sensitivity simulations, with different ice sheet thicknesses. The base point is near Hawaii. (a) 0%, (b) 20%. (c) 40%, (d) 60%, (e) 80%, (f) 100%, (g) 150%, and (h) PIC. The correlation coefficient of 0.35 corresponds to the 95% confidence level for 30-year correlations.

Fig. 3 summarizes correlation coefficients around the four base points for PMIP2, PMIP3, and our sensitivity simulations, according to our definition above. In Fig. 3a, both CCSM3 and CCSM4 show statistically significant correlations at all the four points in the PIC simulations. In contrast, they all demonstrate insignificant correlations near Alberta in LGM simulations. The significant correlation of CCSM4 LGM simulation near the Gulf coast is a result of subtropical wave train (Fig. S4d), as mentioned above. In Fig. 3b, the correlation coefficient near Alberta becomes less significant as ice sheet thickness reaches 80%. Correlation coefficients at the Gulf coast are insignificant for 80% and 150% ice sheet thickness. The significant correlation for 100% ice sheet thickness is a result of subtropical wave train, as shown in Fig. 2f.

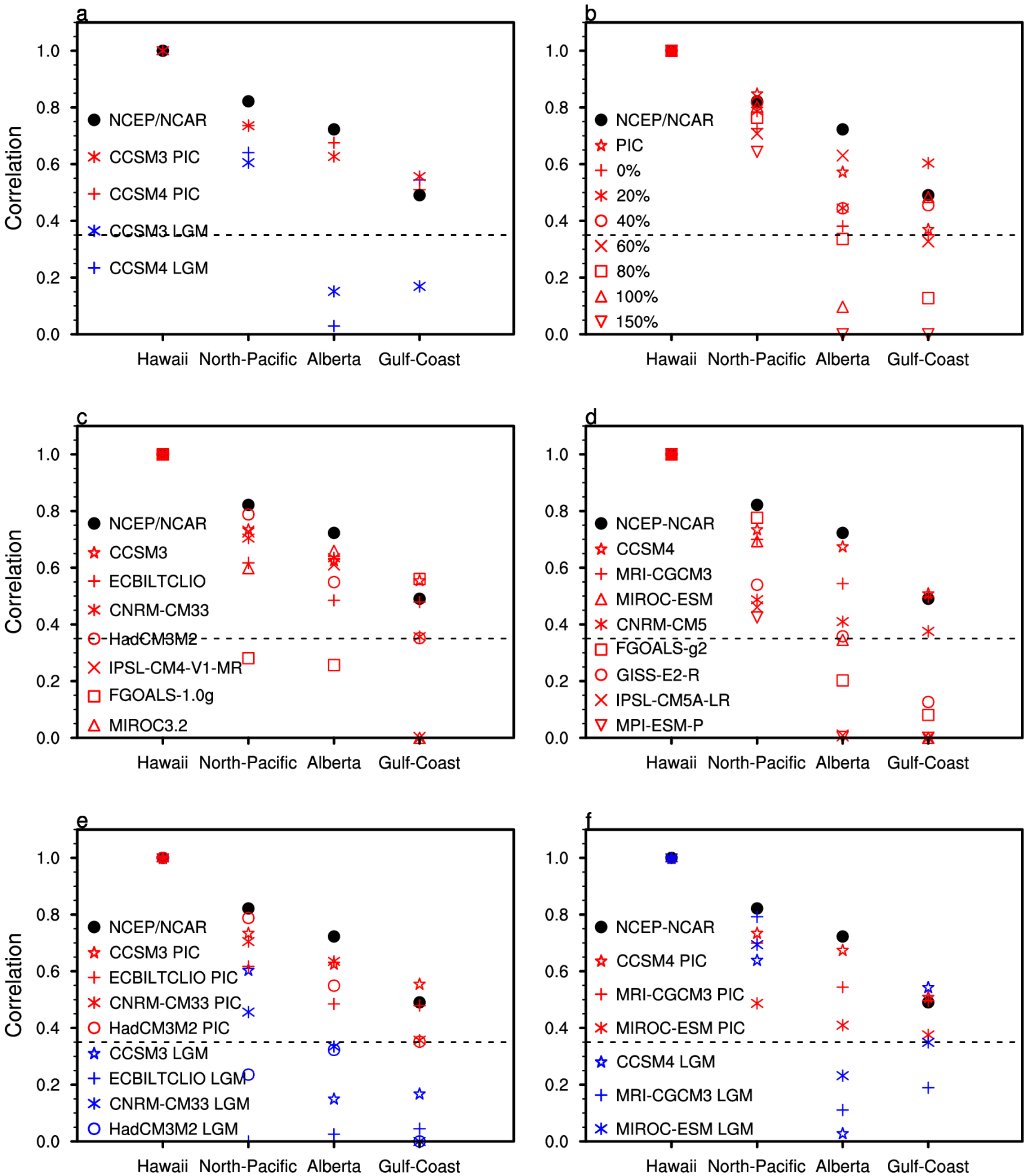

Fig. 3. Correlation coefficients at the four PNA action centers in PIC and LGM simulations for PMIP2 and PMIP3 models, with the base point near Hawaii. The negative values over North Pacific and the Gulf Coast are reversed to positive. The dashed lines correspond to 0.35, which represent the 95% confidence level. (a) CCSM3 and CCSM4, (b) sensitivity simulations, (c) PIC simulations of PMIP2 models, (d) PIC simulations of PMIP3 models, (e) LGM and PIC

simulations for well-performing PMIP2 models, and (f) LGM and PIC simulations for well-performing PMIP3 models.

Figs. 3c and d shows that most PMIP2 and PMIP3 models are able to reproduce the center of negative correlations over the North Pacific in their PIC simulations, except for FGOALS-1.0g. FGOALS-1.0g that generates insignificant correlations at either North Pacific or Alberta. CNRM-CM33 and MIROC3.2 cannot generate significant correlations near the Gulf coast. Fig. 3d shows that CCSM4, MRI-CGCM3, and MIROC-ESM are able to reproduce significant correlations at all four points in their PIC simulations, whereas the other 5 models have insignificant correlations at either Alberta or the Gulf Coast. Figs. 3e and f show that PMIP2 and PMIP3 models, which have good performance in simulating the PNA teleconnection in PIC simulations, all cannot reproduce significant positive correlations at Alberta or even negative correlations near the Gulf coast in the LGM simulations. These results all suggest that the PNA was distorted or broken at LGM.

Because the PNA pattern is characterized by a quasi-stationary wave train from the tropical Pacific to North America, the above simulation results suggest that the PNA wave-train propagation is largely altered at LGM. This can be confirmed by activity fluxes of stationary waves at 500 hPa calculated, using equation 7.1 in Plumb (1985) (Fig. 4), which represents the propagation direction of stationary waves (Plumb, 1985). At present, the wave activity fluxes have two branches for wave propagation from the North Pacific toward North America (Fig. 4a). The major branch propagates northeastward, forming the PNA teleconnection, while the minor branch propagates southeastward. At LGM, however, wave propagation is altered drastically. Wave propagation is deflected toward the subtropics (Figs. 4b and c). This is consistent with the correlation map in Fig. S2i that shows a wave train from North Pacific to the Gulf Coast.

Therefore, the distorted or broken PNA at LGM is mainly due to the deflection of wave propagation toward the southeast.

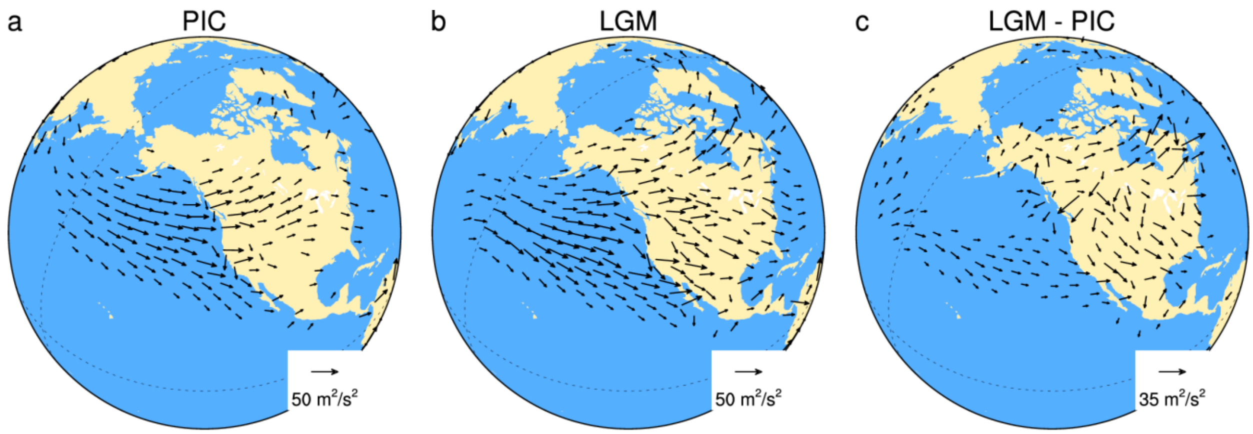

Fig. 4. Stationary wave activity fluxes in PMIP2 CCSM3 simulations at 500 hPa. (a) PIC, (b) LGM, and (c) LGM – PIC. Length scales of wave activity vectors are marked in plots. Wave activity vectors are plotted as their length scales are greater than 12 $m^2\ s^{-2}$ in plots (a) and (b) and 6.5 $m^2\ s^{-2}$ in plot (c). Here, stationary wave activity fluxes are calculated with monthly-mean data.

Wave propagation is oriented by the extratropical wave guide, which in turn is determined by extratropical zonal flows (Hoskins and Karoly, 1981; Jin and Hoskins, 1995). Therefore, the deflection of stationary wave propagation at LGM is caused due to changes in extratropical zonal flows. A comparison of zonal winds between PIC and LGM simulations shows several major differences (Figs. 5a vs. 5b). First, the zonal jet stream is much stronger at LGM than at present. Second, the jet is shifted equatorward at LGM, and the jet is turned southeastward as it approaches the North American continent, in contrast to the northeast orientation at present. Third, similar to that in early studies (Cohmap, 1988; Kutzbach and Wright, 1985; Rind, 1987), the jet splits over North America with the much stronger branch located in the subtropics, leaving the much weaker branch over northern Canada. These features can be seen more clearly in differences of zonal winds between LGM and PIC simulations (Fig. 5c).

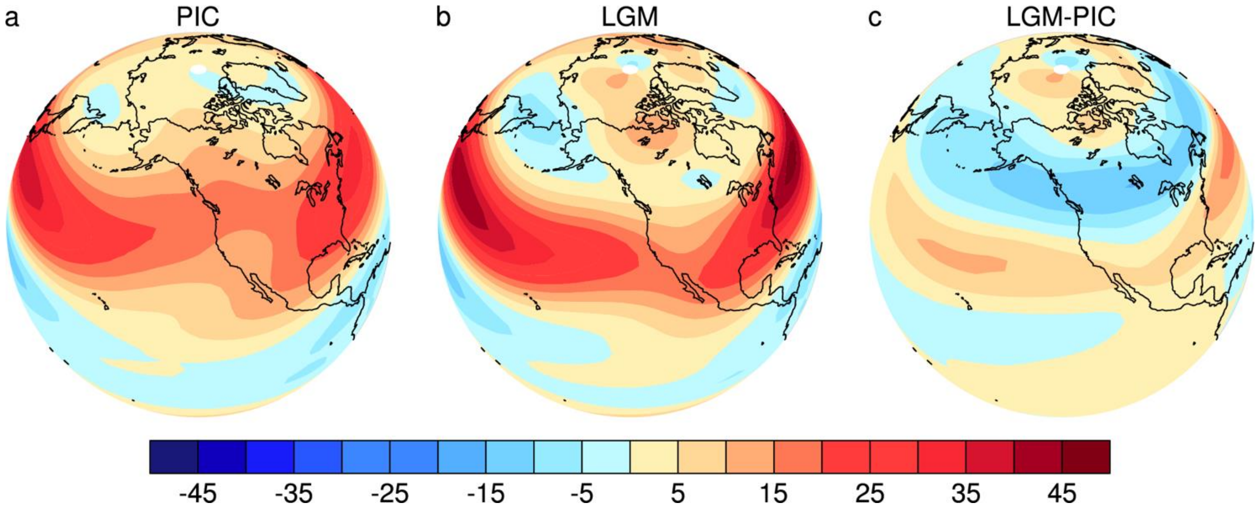

Fig. 5. Maps of 500 hPa zonal winds in DJF in PMIP2 CCSM3 simulations. (a) PIC, (b) LGM, and (c) LGM – PIC. Color interval: 5 m s^{-1}.

Differences of zonal winds over North America can also be illustrated with the vertical cross-sections along 100 °W (Fig. 6). The single subtropical westerly jet in the PIC simulation (Fig. 6b) is split into two jets at LGM (Fig. 6c): a subtropical jet at 30 °N and 200 hPa, and a subpolar jet at 63 °N and between 400 and 300 hPa. The subtropical jet is intensified to a maximum wind speed of 40 m s^{-1} and is located at a lower latitude, and it is much stronger than that in the PIC simulation (~ 30 m s^{-1}). The subpolar jet is much weaker, with a maximum speed of about 12 m s^{-1}. The differences in zonal winds are associated with different thermal structures between LGM and PIC simulations. Comparison of Figs. 6f with 6e shows that latitudinal temperature gradients in the subtropics are sharper at LGM than at present. Thus, the stronger subtropical jet is associated with the sharper temperature gradient.

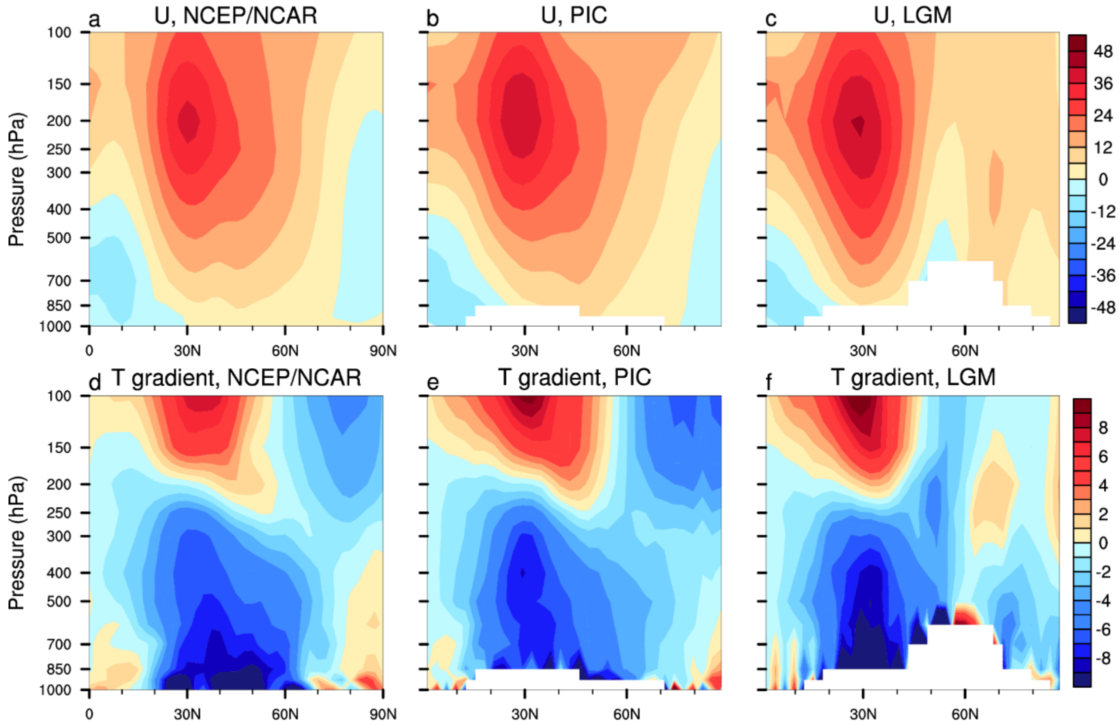

Fig. 6. Vertical cross sections of DJF zonal winds and meridional temperature gradients along the longitude of 100 °W in the NCEP/NCAR reanalysis and PMIP2 CCSM3 simulations. Top panels: zonal winds, and bottom panels: temperature gradients. Left panels: NCEP/NCAR, middle panels: PIC, and right panels: LGM. Zonal-wind unit is ms-1, and temperature gradient unit is K/(1000 km).

The jet split and the equatorward shift of the major jet branch are caused by the orographic forcing of the large and thick Laurentide ice sheet. Fig. S5 shows how the westerly jet responds to the ice sheet thickness in the sensitivity simulations. In the case with 0% ice sheet thickness, there is only a single jet in the subtropics (Fig. S5a), almost the same as that in the PIC simulation. As ice sheet thickness is increased, the jet is strengthened associated with the sharper meridional temperature gradient (Fig. S6), and the core of the jet becomes narrower. Significant jet splitting occurs as ice sheet thickness reaches 80% (Fig. S5e). It is the reason why the distortion of the PNA occurs as ice sheet thickness reaches 80%. As the ice sheet thickness is increased to 100% and 150%, the jet split becomes more significant, and easterly winds begin to develop over the ice sheet.

Note that the orographic forcing is further reinforced by the thermal forcing of the large ice sheet (Liakka, 2012). The high albedo of the ice sheet causes cold air aloft, resulting in sharper latitudinal temperature gradients in the subtropics at LGM. Thus, this enhanced temperature gradient causes a stronger subtropical jet through the thermal wind relation. Our sensitivity simulations also show that subtropical temperature gradients become sharper with increasing ice sheet thicknesses.

The split of the westerly jet acts as wave guides to orient wave propagation, as shown in Fig. 4. The major path of wave propagation is associated with the major jet branch. Both Figs. S2c and S2i all show that a southern wave train is established along the southern jet branch from North Pacific sweeping across the southern US. This wave train would lead to more storms and precipitation in the American Southwest, consistent with proxy records and previous modeling studies (Cohmap, 1988). The minor path of wave propagation toward the Arctic is along with the northern branch (Fig. 1c), but of a much reduced strength. As such, a southern wave guide is established along the subtropical jet, while the northern wave guide is either distorted toward the Arctic or completely broken.

Our sensitivity simulations demonstrate dramatic changes in the PNA wave train between 80% and 100% ice sheet thicknesses (Fig. 2e vs. Fig. 2f). The dramatic changes are associated with the occurrence of easterly winds over the Laurentide ice sheet (Figs. 7a-c). For the case of 80% ice sheet thickness, westerly winds remain between the two jet streams (Fig. 7b). In contrast, easterly winds appear over the ice sheet as the ice sheet thickness is increased to 100% (Fig. 7c). The zero-wind line between easterly and westerly winds acts as the critical layer to reflect stationary waves (Held, 1983). This can be addressed with calculations of critical stationary wavenumbers (Fig. 7 d-f) (eq. 6.29 in Held (1983)). The orange-red shading indicates the areas where stationary waves can propagate, while the shallow-blue shading indicates the areas with imaginary wavenumbers, in which propagation of stationary waves is prohibited. These shallow-blue areas are associated with the easterly winds. When the ice sheet thickness is 60% (Fig. 7d), North Pacific and North America are dominated with positive wavenumbers, and the PNA remains. For 80% ice sheet thickness, imaginary wavenumbers occur in Northeast Pacific and North America (Fig. 7e), and it forces the PNA wave train distorted toward the Arctic. For 100% ice sheet thickness, the subpolar region is dominated with imaginary wavenumbers (Fig. 7f). It causes stationary waves reflected southeastward, leading to the establishment of the southern wave train and the breaking up of the northern wave train.

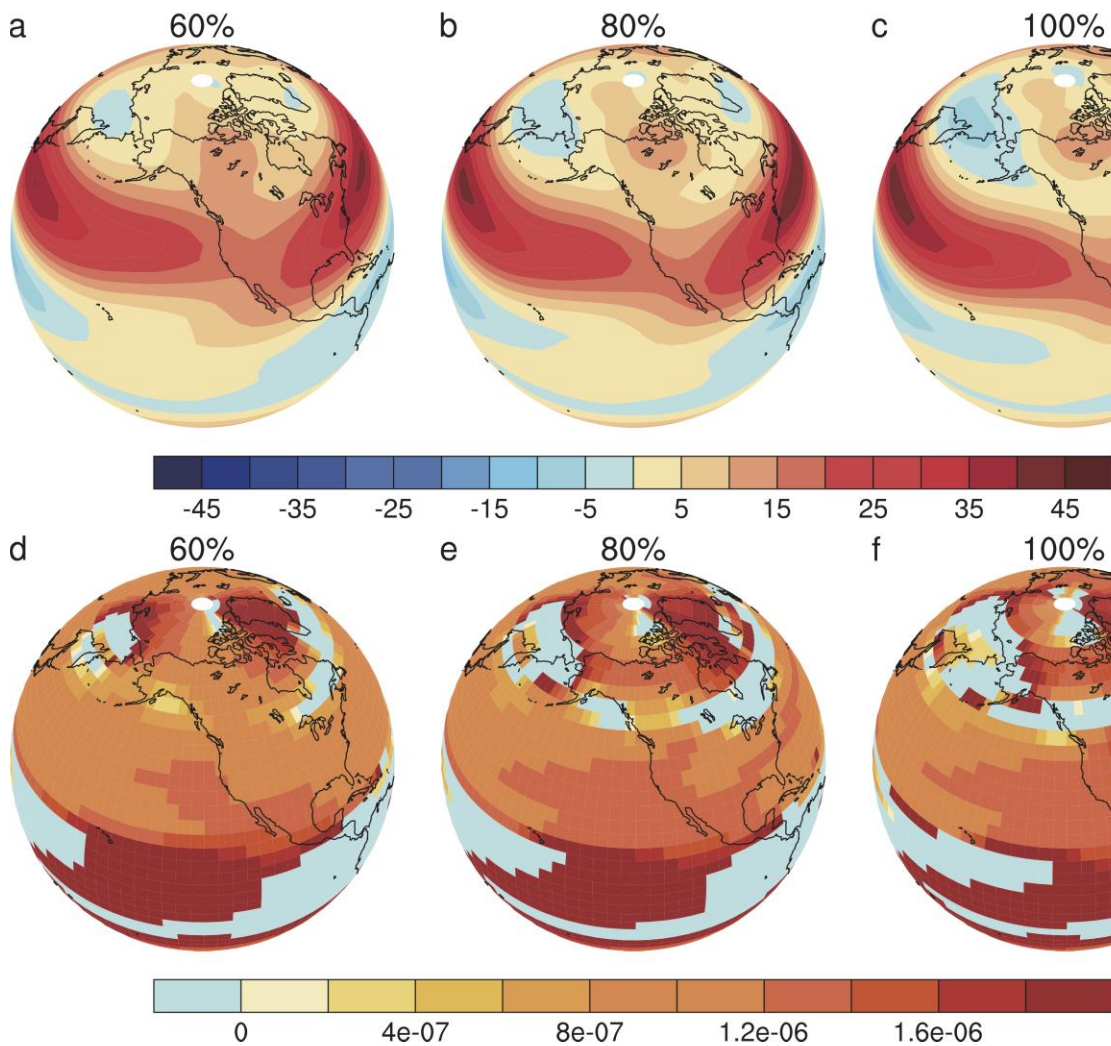

Fig. 7. Distributions of zonal winds and stationary wavenumbers for different ice sheet thicknesses in sensitivity simulations in DJF. Top panels: zonal winds, and bottom panels: stationary wavenumbers. (a, d) 60%, (b, e) 80%, and (c, f) 100%. Zonal-wind unit is $m\ s^{-1}$, and stationary wavenumber unit is m^{-1}. The shallow-blue areas in the bottom panels have imaginary wavenumbers.

The occurrence of easterly winds can be further illustrated with the geopotential heights at 500 hPa (Fig. 8). In both NCEP/NCAR reanalysis and the PIC simulation, there is only a weak ridge along the west coast of North America (Figs. 8a and b). In contrast, the ridge at LGM is largely enhanced and shows northwestern tilting (Fig. 8c). It is this strong ridge that leads to altered zonal flows. The major branch moves equatorward, and the minor branch flows around the ridge northward, resulting in the formation of easterly winds over the ice sheet and North Pacific. It also can be seen in the sensitivity simulations that the west-coast ridge increases with increasing ice sheet thickness (Fig. S7).

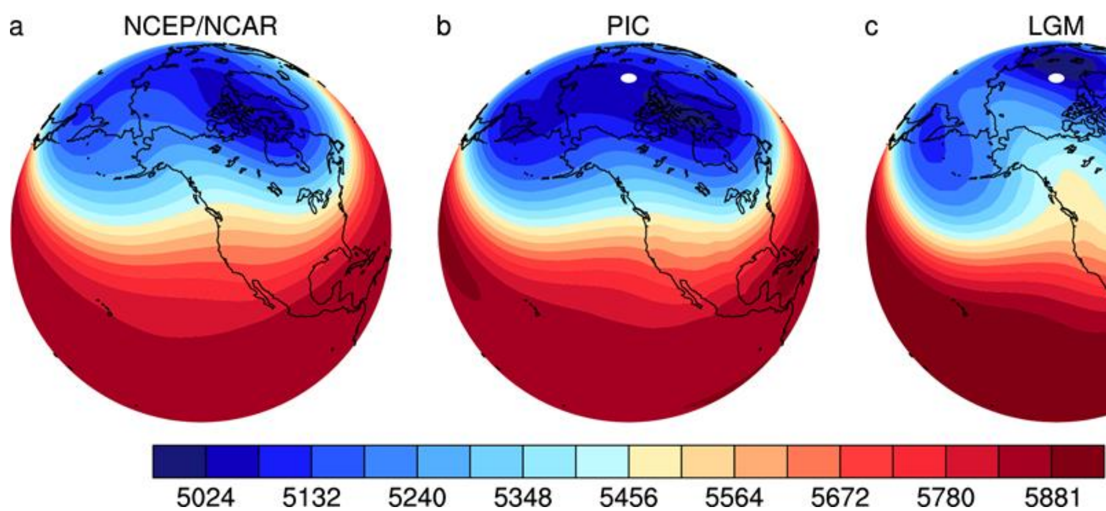

Fig. 8. Climatological mean 500 hPa geopotential heights in DJF in NCEP/NCAR reanalysis and PMIP2 CCSM3 simulations. (a) NCEP/NCAR, (b) PIC, and (c) LGM. The unit is meter.

The distorted or broken PNA teleconnection at LGM suggests a disconnection of climate variability from the tropical Pacific to the North American continent, such that ENSO would have little direct influence on North American climates. Fig. 9 shows regression maps of surface air temperatures (SATs) on the Nino3.4 index in DJF. At present, the remote ENSO impacts on North American SATs through the PNA teleconnection can be identified clearly (Figs. 9a and 9b), which is characterized by an anomalously warm climate over the northwestern North America and an anomalously cold climate over the southeastern United State. However, there are no significant regressions of SATs over North America at LGM (Fig. 9c), except for the positive values near the east coast.

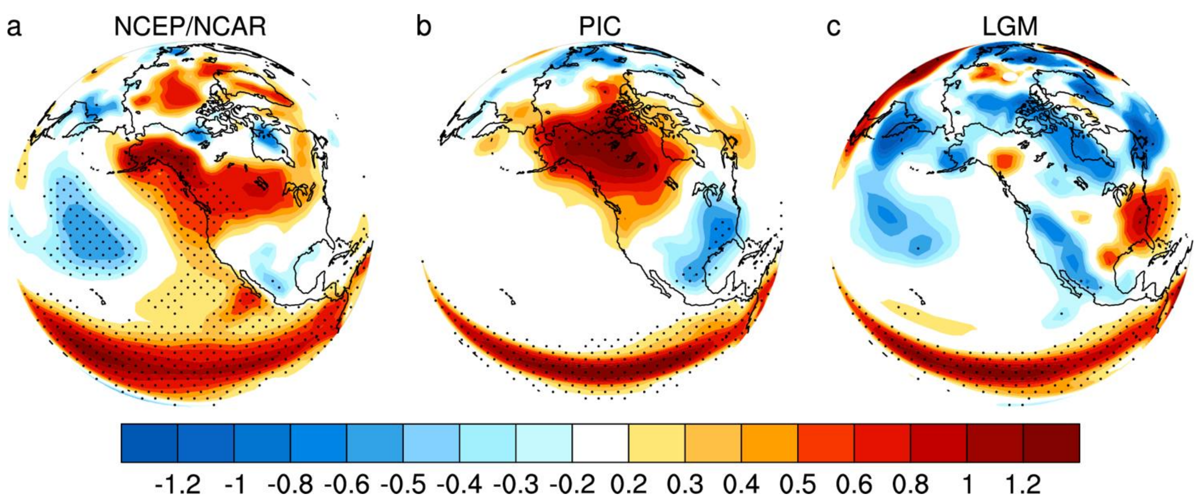

Fig. 9. DJF SAT regressions on the Nino3.4 index in NCEP/NCAR reanalysis and PMIP2 CCSM3 simulations. (a) NCEP/NCAR reanalysis, (b) PIC, and (c) LGM. The regression value of 0.21 corresponds to the 95% confidence level for 30-year regressions.

At present, ENSO also has important influences on North American precipitation. Similar features can also be seen from regression maps of precipitation (Fig. 10). Fig. 10a shows precipitation regression on the Nino3.4 index in the PIC simulation. The wave train pattern of precipitation is clearly shown in the plot. However, the wave train of precipitation is absent in the LGM simulations (Fig. 10b).

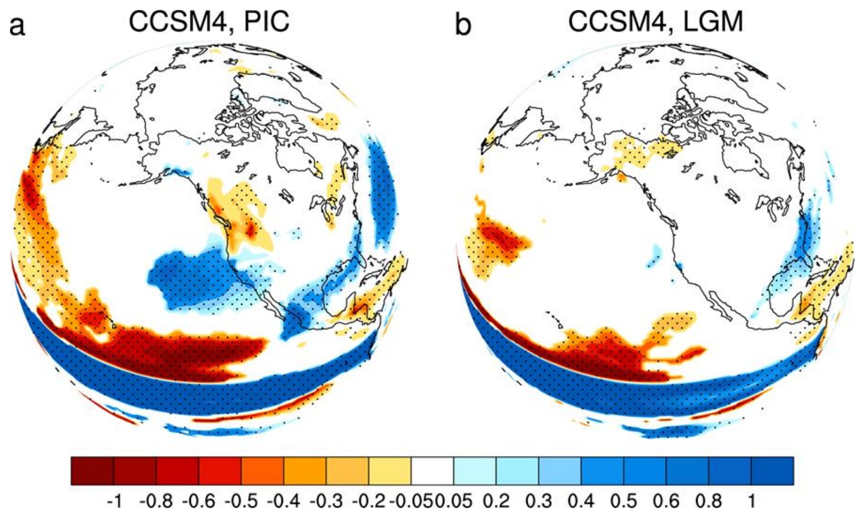

Fig. 10. Precipitation regressions on the Nino3.4 index in the CCSM4 PMIP3 simulations. (a) PIC, and (b) LGM. Dotted areas indicate significant regressions for the 95% confidence level for 30-year regressions.

4 Conclusions and Discussions

We have shown in climate simulations that the large and thick Laurentide ice sheet at LGM forced jet splitting and the formation of easterly winds over North America. It consequently causes altered wave guides and distorted or broken PNA. It appears that the PNA was separated into two teleconnections at LGM. One is from North Pacific to Arctic, and the other one is from North Pacific to the southern part of North America.

This result suggests that ENSO would have little direct influence on North American climates at LGM. Our study provides a dynamic framework to understand the PNA teleconnection not only at LGM but also in other glacial periods. This understanding may help us interpreting proxy records in the past. For example, a previous study on varve record in New England linked the change of the intensity of interannual variability in the northeastern US during the early glacial period to the change of ENSO intensity (Rittenour et al., 2000). Our study suggests that this interannual variability is unlikely to be caused by the climate variability from the tropical Pacific, because of the distorted or broken PNA teleconnection; instead, it reflects mainly the change of local climate variability (Liu et al., 2014). Much further work is needed in developing proxy records of high temporal resolutions to identify the PNA change in paleoclimate records.

Previous works have shown weaker ENSO variability at LGM (Zhu et al., 2017). How the weaker tropical variability would impact climates over extratropics and high-latitudes, through the altered atmospheric teleconnections, deserves future studies.

Acknowledgements

We thank the international modeling groups of the PMIP2 and PMIP3 projects who make the simulation data available. We also thank modeling groups of CMIP3 and CMIP5 whose pre-industry simulation data are used here. NCEP Reanalysis data are provided by the NOAA/OAR/ESRL PSD, Boulder, Colorado, USA, from their Web site at http://www.cdc.noaa.gov/. Y. Hu and Y. Xia are supported by the National Natural Science Foundation of China (NSFC) under grants 41888101 and 41761144072, and Z. Liu is supported by NSFC under grant 41630527. We thank the Editor and two anonymous reviewers for their insightful comments on the paper.

References

Abe-Ouchi, A., Saito, F., Kageyama, M., Braconnot, P., Harrison, S. P., Lambeck, K., Otto-Bliesner, B. L., Peltier, W. R., Tarasov, L., Peterschmitt, J. Y., and Takahashi, K.: Ice-sheet configuration in the CMIP5/PMIP3 Last Glacial Maximum experiments, Geosci. Model Dev., 8, 3621-3637, 2015.

Allan, A. M., Hostetler, S. W., and Alder, J. R.: Analysis of the present and future winter Pacific-North American teleconnection in the ECHAM5 global and RegCM3 regional climate models, Climate Dynamics, 42, 1671-1682, 2014.

Braconnot, P., Harrison, S. P., Kageyama, M., Bartlein, P. J., Masson-Delmotte, V., Abe-Ouchi, A., Otto-Bliesner, B., and Zhao, Y.: Evaluation of climate models using palaeoclimatic data, Nature Climate Change, 2, 417, 2012.

Braconnot, P., Otto-Bliesner, B., Harrison, S., Joussaume, S., Peterchmitt, J. Y., Abe-Ouchi, A., Crucifix, M., Driesschaert, E., Fichefet, T., Hewitt, C. D., Kageyama, M., Kitoh, A., Laîné, A., Loutre, M. F., Marti, O., Merkel, U., Ramstein, G., Valdes, P., Weber, S. L., Yu, Y., and Zhao, Y.: Results of PMIP2 coupled simulations of the Mid-Holocene and Last Glacial Maximum – Part 1: experiments and large-scale features, Clim. Past, 3, 261-277, 2007.

Chen, Z., Gan, B., Wu, L., and Jia, F.: Pacific-North American teleconnection and North Pacific Oscillation: historical simulation and future projection in CMIP5 models, Climate Dynamics, doi: 10.1007/s00382-017-3881-9, 2017. 2017.

Clark, P. U., Dyke, A. S., Shakun, J. D., Carlson, A. E., Clark, J., Wohlfarth, B., Mitrovica, J. X., Hostetler, S. W., and McCabe, A. M.: The Last Glacial Maximum, Science, 325, 710-714, 2009.

Clark, P. U. and Mix, A. C.: Ice sheets and sea level of the Last Glacial Maximum, Quaternary Science Reviews, 21, 1-7, 2002.

Cohmap, M.: Climatic Changes of the Last 18,000 Years: Observations and Model Simulations, Science, 241, 1043-1052, 1988.

Collins, W. D., Bitz, C. M., Blackmon, M. L., Bonan, G. B., Bretherton, C. S., Carton, J. A., Chang, P., Doney, S. C., Hack, J. J., Henderson, T. B., Kiehl, J. T., Large, W. G., McKenna, D. S., Santer, B. D., and Smith, R. D.: The Community Climate System Model Version 3 (CCSM3), Journal of Climate, 19, 2122-2143, 2006.

Held, I. M.: Stationary and Quasi-stationary Eddies in the Extratropical Troposphere: Theory. In: Large-scale Dynamical Processes in the Atmosphere, B. J. Hoskins and Pearce, R. P. (Eds.), Academic Press, 1983.

Held, I. M., Ting, M., and Wang, H.: Northern Winter Stationary Waves: Theory and Modeling, Journal of Climate, 15, 2125-2144, 2002.

Henderson, K. G. and Robinson, P. J.: Relationships between the pacific/north american teleconnection patterns and precipitation events in the south - eastern USA, International Journal of Climatology, 14, 307-323, 1994.

Horel, J. D. and Wallace, J. M.: Planetary-Scale Atmospheric Phenomena Associated with the Southern Oscillation, Monthly Weather Review, 109, 813-829, 1981.

Hoskins, B. J. and Karoly, D. J.: The Steady Linear Response of a Spherical Atmosphere to Thermal and Orographic Forcing, Journal of the Atmospheric Sciences, 38, 1179-1196, 1981.

Jin, F. and Hoskins, B. J.: The Direct Response to Tropical Heating in a Baroclinic Atmosphere, Journal of the Atmospheric Sciences, 52, 307-319, 1995.

Jones, T. R., Roberts, W. H. G., Steig, E. J., Cuffey, K. M., Markle, B. R., and White, J. W. C.: Southern Hemisphere climate variability forced by Northern Hemisphere ice-sheet topography, Nature, 554, 351, 2018.

Justino, F. and Peltier, W. R.: The glacial North Atlantic Oscillation, Geophysical Research Letters, 32, 2005.

Justino, F., Timmermann, A., Merkel, U., and Souza, E. P.: Synoptic Reorganization of Atmospheric Flow during the Last Glacial Maximum, Journal of Climate, 18, 2826-2846, 2005.

Kistler, R., Kalnay, E., Collins, W., Saha, S., White, G., Woollen, J., Chelliah, M., Ebisuzaki, W., Kanamitsu, M., Kousky, V., van den Dool, H., Jenne, R., and Fiorino, M.: The NCEP-NCAR 50-year reanalysis: Monthly means CD-ROM and documentation, B Am Meteorol Soc, 82, 247-267, 2001.

Kutzbach, J. E. and Wright, H. E.: Simulation of the climate of 18,000 years BP: Results for the North American/North Atlantic/European sector and comparison with the geologic record of North America, Quaternary Science Reviews, 4, 147-187, 1985.

Laîné, A., Kageyama, M., Salas-Mélia, D., Voldoire, A., Rivière, G., Ramstein, G., Planton, S., Tyteca, S., and Peterschmitt, J. Y.: Northern hemisphere storm tracks during the last glacial maximum in the PMIP2 ocean-atmosphere coupled models: energetic study, seasonal cycle, precipitation, Climate Dynamics, 32, 593-614, 2009.

Lau, N.-C.: Interactions between Global SST Anomalies and the Midlatitude Atmospheric Circulation, B Am Meteorol Soc, 78, 21-34, 1997.

Leathers, D. J., Yarnal, B., and Palecki, M. A.: The Pacific/North American Teleconnection Pattern and United States Climate. Part I: Regional Temperature and Precipitation Associations, Journal of Climate, 4, 517-528, 1991.

Li, C. and Battisti, D. S.: Reduced Atlantic Storminess during Last Glacial Maximum: Evidence from a Coupled Climate Model, Journal of Climate, 21, 3561-3579, 2008.

Liakka, J.: Interactions between topographically and thermally forced stationary waves: implications for ice-sheet evolution, Tellus A: Dynamic Meteorology and Oceanography, 64, 11088, 2012.

Liu, Z., Lu, Z., Wen, X., Otto-Bliesner, B. L., Timmermann, A., and Cobb, K. M.: Evolution and forcing mechanisms of El Niño over the past 21,000 years, Nature, 515, 550, 2014.

Löfverström, M., Caballero, R., Nilsson, J., and Messori, G.: Stationary wave reflection as a mechanism for zonalizing the Atlantic winter jet at the LGM, J. Atmos. Sci., 73, 3329-3342, 2016.

Lü, J.-M., Kim, S.-J., Abe-Ouchi, A., Yu, Y., and Ohgaito, R.: Arctic Oscillation during the Mid-Holocene and Last Glacial Maximum from PMIP2 Coupled Model Simulations, Journal of Climate, 23, 3792-3813, 2010.

Magnusdottir, G. and Haynes, P. H.: Reflection of planetary waves in three-dimensional tropospheric flows, J. Atmos. Sci., 56, 652-670, 1999.

Marshall, S. J., James, T. S., and Clarke, G. K.: North American ice sheet reconstructions at the Last Glacial Maximum, Quaternary Science Reviews, 21, 175-192, 2002.

Otto-Bliesner, B. L., Brady, E. C., Clauzet, G., Tomas, R., Levis, S., and Kothavala, Z.: Last Glacial Maximum and Holocene Climate in CCSM3, Journal of Climate, 19, 2526-2544, 2006.

Peltier, W. R.: Global glacial isostasy and the surface of the ice-age Earth: The ICE-5G (VM2) model and GRACE, Annual Review of Earth and Planetary Sciences, 32, 111-149, 2004.

Plumb, R. A.: On the Three-Dimensional Propagation of Stationary Waves, Journal of the Atmospheric Sciences, 42, 217-229, 1985.

Rind, D.: Components of the ice age circulation, Journal of Geophysical Research: Atmospheres, 92, 4241-4281, 1987.

Rittenour, T. M., Brigham-Grette, J., and Mann, M. E.: El Niño-Like Climate Teleconnections in New England During the Late Pleistocene, Science, 288, 1039-1042, 2000.

Rivière, G., Laîné, A., Lapeyre, G., Salas-Mélia, D., and Kageyama, M.: Links between Rossby Wave Breaking and the North Atlantic Oscillation–Arctic Oscillation in Present-Day and Last Glacial Maximum Climate Simulations, Journal of Climate, 23, 2987-3008, 2010.

Sherriff-Tadano, S. and Itoh, H.: Teleconnection Patterns Appearing in the Streamfunction Field, SOLA, 9, 115-119, 2013.

Straus, D. M. and Shukla, J.: Does ENSO Force the PNA?, Journal of Climate, 15, 2340-2358, 2002.

Wallace, J. M. and Gutzler, D. S.: Teleconnections in the Geopotential Height Field during the Northern Hemisphere Winter, Monthly Weather Review, 109, 784-812, 1981.

Yanase, W. and Abe-Ouchi, A.: The LGM surface climate and atmospheric circulation over East Asia and the North Pacific in the PMIP2 coupled model simulations, Clim. Past, 3, 439-451, 2007.

Yanase, W. and Abe-Ouchi, A.: A Numerical Study on the Atmospheric Circulation over the Midlatitude North Pacific during the Last Glacial Maximum, Journal of Climate, 23, 135-151, 2010.

Yeager, S. G., Shields, C. A., Large, W. G., and Hack, J. J.: The Low-Resolution CCSM3, Journal of Climate, 19, 2545-2566, 2006.

Zhu, J., Liu, Z., Brady, E., Otto-Bliesner, B., Zhang, J., Noone, D., Tomas, R., Nusbaumer, J., Wong, T., Jahn, A., Tabor, C.: Reduced ENSO variability at the LGM revealed by an isotope-enabled Earth system model. Geophysical Research Letters 44, 6984-6992, 2017.